Ordering in the mixed $ZnGeN_2$-GaN alloy system: Crystal structures and band structures of $ZnGeGa_2N_4$ from first principles

Benthara Hewage Dinushi Jayatunga, Sai Lyu, Santosh Kumar Radha, Kathleen Kash, and Walter R. L. Lambrecht
Department of Physics, Case Western Reserve University, 10900 Euclid Avenue, Cleveland, Ohio 44106-7079, USA

(Received 22 June 2018; revised manuscript received 12 August 2018; published 26 November 2018)

While $ZnGeN_2$ and GaN are closely lattice matched and have almost equal band gaps around 3.5 eV, their band offset is of order 1 eV. This situation suggests that there could be an opportunity for tuning the band gap in the alloy system. In particular, we examine here the 50 at. % composition, $ZnGeGa_2N_4$. It is shown that there are two 16-atom unit cell ordered structures, with space groups $Pmn2_1$ and $P1n1$, that obey the octet rule, with each N bound to two Ga, one Zn, and one Ge. The $Pmn2_1$ structure is a superlattice along the orthorhombic b direction of the $ZnGeN_2$ $Pbn2_1$ structure, in which half the cell is replaced by GaN; consequently, octet-rule-preserving polytypes spanning the entire range of composition can be formed based upon this structure. Two other structures that do not obey the octet rule are also considered for comparison. These are superlattices consisting of 1/2 cell GaN and 1/2 cell $ZnGeN_2$ along the orthorhombic a or c direction. By means of fully relaxed density functional calculations, we find that the structures that obey the octet rule have significantly lower total energy than the ones that do not. Detailed crystallographic data on these four structures: space group, lattice constants, relaxed Wyckoff positions, and predicted x-ray diffraction spectra, are provided. The lowest energy structure is found to have a negative energy of formation, comparable to those of $ZnGeN_2$ and GaN. However, the mixing energy is slightly positive, indicating a tendency toward phase separation into $ZnGeN_2$ and GaN even when only considering low energy octet-rule-preserving structures. The band gaps of the octet-rule-preserving structures, calculated using the quasiparticle self-consistent GW method, are found to be slightly higher than those of $ZnGeN_2$ and GaN. This result can be explained in terms of size quantization effects compensating the reduced interface band gap.

DOI: 10.1103/PhysRevMaterials.2.114602

I. INTRODUCTION

Alloying between different elements is one of the oldest approaches to engineering desired materials properties. Alloying among isovalent elements of binary semiconductors, e.g., $Al_xGa_{1-x}As$, is the primary method used to tailor band gaps. However, as we go down any column in the periodic table, the size of the atom increases, and hence this type of alloying is in general, with a few notable exceptions, accompanied by large changes in lattice constant. This situation often leads to limitations in epitaxial growth because of lattice mismatch, although creating alloys involving both cations and anions, e.g., $In_xGa_{1-x}As_yP_{1-y}$, can introduce additional flexibility to tune the lattice matching while varying the band gap, a flexibility that has been crucial in developing semiconductor devices for optical communications. Another, less studied route to flexibility in tailoring semiconductor materials properties is to alloy families of heterovalent ternary compounds with each other and with the binary compounds. In the particular case of group-III nitrides, compounds related to the binary nitrides are formed by replacing every pair of Ga atoms (group III) by an element from group II and group IV, e.g., $ZnGeN_2$ in an ordered manner so as to preserve the octet rule. Many of these compounds have lattices based on the binary wurtzite lattice and thus might be readily alloyed with the III-nitrides, or grown with them in heterostructures. We have reported on the band structures and phonons in Zn-IV-N_2 [1–4], Mg-IV-N_2 [5,6], and Cd-IV-N_2 [7,8] and on the growth of $ZnGeN_2$ [9,10] and of $ZnSnN_2$ [11,12]. Raman spectroscopy studies of the phonons were presented in Refs. [13,14]. Point defects in $ZnGeN_2$ were studied by Skachkov *et al.* [15–17] and Adamski *et al.* [18]. An overview of the literature on these materials up to 2013 can be found in Ref. [19], for more up-to-date information in the above cited papers, and in a recent review article of both wurtzite-based and zinc-blende-based heterovalent ternary compounds [20]. $ZnGeN_2$ and $ZnSnN_2$ and their alloys have attracted increased recent interest, including for their potential as solar photovoltaic materials [21–29] and, in combination with the III-nitrides, for the design of efficient green and longer wavelength III-nitride light-emitting diode structures [30,31]. Here we consider the alloys between II-IV-N_2 and III-N.

While $ZnGeN_2$ and GaN have almost identical band gaps around 3.4 eV, and in addition have the attractive attribute of close lattice matching, a significant band offset has been predicted [32]. The valence band offset (VBO) is predicted to be 1.2–1.3 eV, depending on crystallographic direction, with the valence band maximum (VBM) of $ZnGeN_2$ lying above that of GaN [33]. This large offset is associated with the effect of the Zn-3d bands on the VBM: the Zn-3d bands lie significantly closer to the VBM than do the Ga-3d and hence have a stronger hybridization effect, which pushes the VBM to higher energy. This type-II staggered band offset suggests that, in a heterostructure composed of the two materials, the interface gap between the conduction band minimum (CBM)

of the GaN regions and the VBM of $ZnGeN_2$ could be lowered by around 1 eV. In an intermixed system or alloy, one could expect that this $ZnGeN_2$-like character of the VBM and GaN-like character of the CBM would be maintained, at least to some extent, and hence a smaller gap than either of the two could be obtained. If we can really lower the gap from 3.4 eV by about 1 eV, we could potentially reach the visible range down to the blue or even green part of the spectrum. Several questions need to be considered. First, are such alloys thermodynamically possible, i.e., what is their energy of formation? Second, if they are feasible, can they still be considered as ultrathin superlattices such that the concept of band offset remains valid? And, if so, what are the size-quantization effects on the bands in such very thin superlattices? The size quantization effects could be expected to increase the gap, so the ultimate values of the gaps of the ordered alloys would be a compromise between band offset and size quantization. Finally, what would be the effect of the real-space indirectness of the gap on the efficiency of light emission in such systems?

In this paper, we do not claim to provide a full set of answers to these questions but provide initial computational insights by focusing on the 50% composition of this alloy system, $ZnGeGa_2N_4$. We assume that the underlying crystal structure remains the wurtzite-like III-N lattice and consider the ordering of Ga substitutions within the two ordered $ZnGeN_2$ orthorhombic structures to search for new ordered crystal structures.

We anticipate that it will be important for the stability of such structures to maintain the octet rule. Therefore, every N should be surrounded by exactly two Ga, one Zn, and one Ge. We consider the two minimal unit cells of 16 atoms and 8 atoms of, respectively, the $Pbn2_1$ and $Pmc2_1$ structures of $ZnGeN_2$ as starting points. (The latter structure has a lower calculated band gap and higher energy of formation than the first, and has not been observed) [12]. By inspection, we find two crystal structures for $ZnGeGa_2N_4$ that satisfy this requirement as described in Sec. III A. One of these, the $Pmn2_1$ structure, is a superlattice consisting of half a cell of $ZnGeN_2$ with half a cell of GaN along the b direction of the $Pbn2_1$ structure. We denote this structure as $[010]_{1/2}$, indicating the direction of the ordering vector and the period with respect to the $Pbn2_1$ unit cell. We also examine the $[100]_{1/2}$ and $[001]_{1/2}$ superlattices. These do not obey the octet rule but they provide a convenient point of comparison for evaluating the importance of the octet rule. From examination of the $Pbn2_1$ structure, it becomes clear that other octet-rule-satisfying alloy compositions, such as 25%–75%, can be formed by constructing appropriate superlattices, inserting different size sections of $ZnGeN_2$ and GaN along the [010] direction of $Pbn2_1$.

We then study the energies of mixing and energies of formation of the various $ZnGeGa_2N_4$ models constructed after relaxing their structural parameters in Sec. III B and their electronic band structures in Sec. III D. We also predict the x-ray diffraction (XRD) spectra of the various structural models in Sec. III C. The results on the band structure are discussed in terms of a Kronig-Penney model in Sec. III E.

As an aside, we mention that similar compositional ternaries and quaternaries can also be envisioned starting from II-VI compounds such as ZnO. In that case the ternary is a I-III-VI_2 compound such as $LiGaO_2$ [34,35]. Indeed, mixed alloy systems of ZnO and $LiGaO_2$, including possibly a new ordered structure at the 50% composition, $LiGaZn_2O_4$, have been reported [36,37]. A full description of the crystallographic structure of that compound, however, has not yet been reported. Very recently, quaternary $ZnGeN_2$-GaN alloys were synthesized in powder form by a gas reduction nitridation method [38]. These results indicated that beyond 10% addition of Ga, the cations became completely disordered, thus yielding a disordered wurtzite structure, and indicating a band gap of 3.02 eV for the 50% case.

II. COMPUTATIONAL METHOD

Density functional theory is used in the local density approximation (LDA) [39] and generalized gradient approximation (GGA) [40] to minimize the total energy of the structures as a function of the lattice constants and atomic positions in the cell. The full-potential linearized muffin-tin orbital method (LMTO), as implemented in the LMF code [41], is used to solve the Kohn-Sham equations self-consistently and calculate the total energy [42,43]. Usually, to minimize a crystal structure as a function of the lattice constants, the stress tensor is used. The latter has not yet been implemented in the LMTO code used here. However, the total energy can be minimized as a function of the lattice constants, while minimizing the energy as a function of atomic positions within the cell, using the forces calculated by means of the LMTO force theorem, for each set of lattice constants, using an algorithm that does not rely on the ability to calculate gradients as a function of the lattice constants. Specifically, we use an efficient genetic algorithm [44] that allows us to minimize the energy to within the required precision in a small number of steps, of order 10–20. The method was tested by comparison to a minimization based on finding the zero stress approach using the ABINIT code [45] with norm-conserving pseudopotentials [46]. Both approaches gave almost identical Wyckoff positions and ratios of the orthorhombic lattice constants. In the end, we performed one last minimization over volume using the LMF code, keeping the reduced coordinates and lattice constant ratios fixed. The ABINIT and LMF codes used in this way gave structures in agreement with each other to within numerical precision. Because the LDA and GGA were previously found to give almost identical reduced coordinates and lattice constant ratios, but different volumes, we relaxed the volumes both in LDA and GGA, finding that the first typically gives a slight underestimate and the latter a slight overestimate. Thus, we can bracket the expected experimental volume between these two values. The changes in band gap with volume, or band gap deformation potentials, were evaluated.

To calculate the energy band structures, we went beyond LDA and GGA by using the quasiparticle self-consistent GW self-energy method (QSGW) [47,48]. The latter is based on Hedin's many-body-perturbation theory [49,50] in the GW approximation (GWA), in which the self-energy is written schematically as $\Sigma = iGW$, with G the one-electron Green's function and W the screened Coulomb interaction, calculated in the random-phase approximation $W = v + vPW$ with

$P = iGG$, in which v is the bare Coulomb interaction and P the irreducible polarization function. However, instead of the usual single shot approach (G_0W_0) to evaluate the effect on the quasiparticle energies by the perturbation $\Sigma - v_{\rm xc}$ in first-order perturbation theory, starting from an arbitrary starting point such as LDA, this method adjusts the static exchange correlation potential of the starting point independent electron Kohn-Sham Hamiltonian H_0 by adding a nonlocal but energy independent $\Delta v_{\rm xc} = \bar{\Sigma} - v_{\rm xc}^{\rm LDA}$ extracted from the dynamic self-energy $\Sigma(\omega)$, and given in terms of its matrix elements in the basis of the H_0 Hamiltonian eigenstates, by

$$\bar{\Sigma}_{ij} = \tfrac{1}{2}\mathrm{Re}\{\Sigma_{ij}(\epsilon_i) + \Sigma_{ij}(\epsilon_j)\}. \quad (1)$$

This approach keeps the quasiparticle equation Hermitian with real eigenvalues because only the Hermitian part of the self-energy is included. After iterating this to self-consistency, the quasiparticle energies become identical to the eigenvalues of the H_0 Hamiltonian. The Hamiltonian includes the full self-energy matrix, not only the diagonal elements, and hence the rediagonalization of the new H_0 Hamiltonian in each iteration can admix the original LDA states. However, instead of making the full Green's function and dynamical self-energy self-consistent, only the quasiparticle energies become self-consistent (hence the name of the approach). In principle, one may then still evaluate the full dynamical self-energy and obtain the imaginary part of the quasiparticles, giving their lifetime, as well as any satellite or other incoherent parts of the excitation, although for semiconductors this result is usually of less interest.

In practice (see details in Ref. [48]), the self-energy matrix is approximated by a diagonal average value above a certain energy (in our case greater than 3 Ry above the VBM). The GW operator equations are solved in matrix form by means of an auxiliary basis, known as the "mixed product basis." It includes interstitial plane waves and products of muffin-tin orbitals in the muffin-tin spheres. The convergence of various cutoff parameters were evaluated at the start of the study. A well-converged basis set was used including two (κ, R_{sm}) (smoothed Hankel function decay parameters) up to angular momenta $spdf$-spd on Zn and $spdf$-sp on Ge, Ga, and N as well as the Ga and Ge $3d$ semicore states treated as local orbitals (confined to their own muffin-tin spheres). The cutoffs for the interstitial plane waves of the Hamiltonian and auxiliary basis sets were set at 3 Ry, and self-energies were calculated up to 3.5 Ry.

A $3 \times 3 \times 3$ GW $\mathbf{k}_m$-point set was found necessary to converge the gaps to the same precision as a well-converged $6 \times 6 \times 4$ set in the wurtzite GaN case. This GW $\mathbf{k}_m$-point mesh is the mesh on which the self-energy $\bar{\Sigma}(\mathbf{k}_m)$ is calculated. To obtain the gaps at arbitrary $\mathbf{k}$ points in the Brillouin zone, or along the symmetry lines, an effective interpolation is used in terms of the atom-centered muffin-tin orbitals. These allow one to construct a real-space representation of the $\Sigma_{\mathbf{R},\mathbf{R}'+\mathbf{T}}$ by a discrete Fourier transform with $\mathbf{R}$ the sites in the cell and $\mathbf{T}$ the periodic lattice vectors, from which a Bloch sum gives back the $\Sigma(\mathbf{k})$ at any $\mathbf{k}$ point, not necessarily on the mesh $\mathbf{k}_m$. Hence,we can obtain the bands at a fine $\mathbf{k}$ mesh along the symmetry lines, and the effective masses, accurately at the GW level.

One of the remaining shortcomings of the GWA in the random-phase approximation is the underscreening due to the omission of electron-hole interactions or ladder diagrams in the calculation of the polarization function. This effect has been found to lead to an underestimate of about 20% on the macroscopic electronic dielectric constant ε_∞ and an overestimate of the gap correction beyond LDA, or the self-energy, by about 20% and can hence be remedied by including only 80% of the Δv_{xc}. This is known as the 0.8Σ approximation [51–53]. For completeness' sake, we will here report the LDA, the full QSGW, and the 0.8Σ gaps.

III. RESULTS

A. Crystal structures

We start from the $Pbn2_1$ structure of $ZnGeN_2$, shown in Fig. 1(a). This structure has a 16-atom orthorhombic unit cell related to the underlying wurtzite structure by $a = 2a_w$ (a_w, c_w are the lattice constants of hexagonal wurtzite), $b \approx \sqrt{3}a_w$, and $c = c_w$. While often labeled $Pna2_1$, with our choice of $a > b > c$ its proper nomenclature is $Pbn2_1$ because the b-type glide mirror plane with translation by $b/2$ is perpendicular to the a direction, its double glide plane n with translations by $a/2$ and $c/2$ is perpendicular to the b direction, and the twofold screw axis is along the c direction. We now replace Ge and Zn atoms by Ga in such a way that each N is bonded to exactly one Zn, one Ge, and two Ga, thus satisfying the octet rule. It is easy to see by inspection that one way to do this is shown in Fig. 1(c). As mentioned in the Introduction, this structure can be described as a $[010]_{1/2}$ superlattice. Its space group is $Pmn2_1$ (No. 31 or C_{2v}^7) because

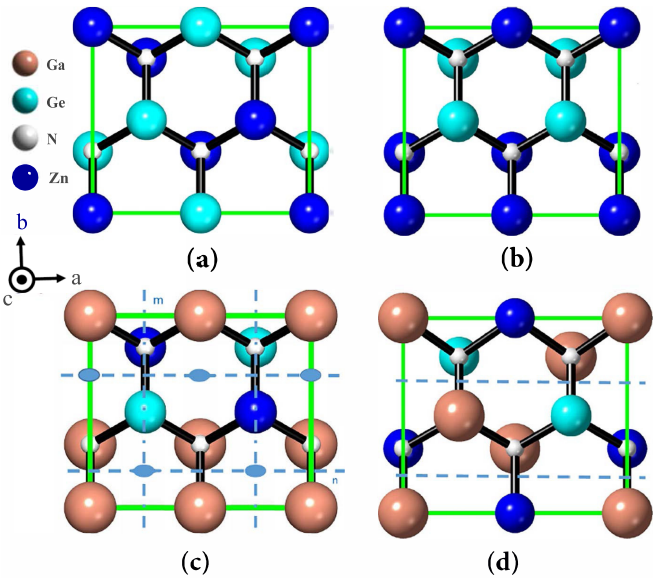

FIG. 1. Octet-rule-preserving $ZnGeGa_2N_4$ structures and their relation to the $ZnGeN_2$ structures with (a) $Pbn2_1$. (b) $Pmc2_1$, (c) $Pmn2_1$, and (d) $P1n1$ space groups. Dark-blue spheres: Zn; light-blue: Ge; slightly larger beige: Ga; and small white spheres: N. The dashed horizontal lines indicate the n-type mirror plane, the dash-dotted vertical lines, the m-type mirror plane, and the ovals the twofold screw axes.

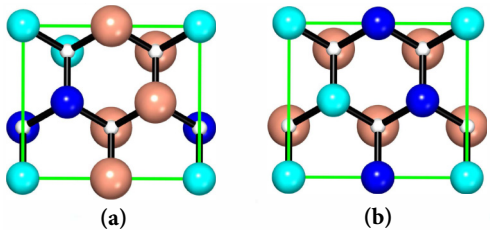

FIG. 2. Non-octet-rule-preserving $ZnGeGa_2N_4$ structures: (a) $[100]_{1/2}$ and (b) $[001]_{1/2}$ superlattices, based on the $Pbn2_1$ $ZnGeN_2$ structure.

the mirror plane perpendicular to **a** is now an ordinary mirror plane instead of a glide mirror plane. The Zn and Ge atoms occur in the $2a$ and the Ga in the $4b$ Wyckoff positions.

The second octet-rule-preserving structure is obtained either from the $Pmc2_1$ structure, shown in Fig. 1(b) or from the $Pbn2_1$ structure, by a different substitution of atoms by Ga. One may notice that Fig. 1(d) indeed overlaps directly with Fig. 1(b) without reshuffling the Zn and Ge atoms and with Fig. 1(a) after a shift of the unit cell origin by $a/2$. The $Pmc2_1$ structure has a unit cell of only eight atoms with $a = a_w$, $b \approx \sqrt{3}a_w$, and $c = c_w$. Here we double that cell along a back to a 16-atom cell and then replace some of the Zn and Ge atoms by Ga in the pattern shown in Fig. 1(d). This structure has only one type of mirror plane, an n-type glide mirror plane. Its space group, $P1n1$ (No. 7, or C_s^2), therefore belongs to the monoclinic crystal system even though the lattice vectors are still orthogonal to each other. This structure, unlike the first, cannot be described as a simple superlattice of alternating GaN and $ZnGeN_2$ blocks. Instead, we see two consecutive (horizontal or a rows) of Zn-Ga mixed character, then two of Ge-Ga mixed character.

These are the only two octet-rule-conserving structures one can form within a 16-atom cell. For comparison, we show the structures which can be described as $[100]_{1/2}$ and $[001]_{1/2}$ in Fig. 2. In both of these cases, the tetrahedra surrounding a N atom are Zn_2GeGa, $ZnGe_2Ga$, Ga_3Zn, and Ga_3Ge instead of the desired $ZnGeGa_2$. The corners of the last octet-rule-preserving tetrahedron have in total a valence of $2 + 4 + 6 = 12$ but each cation is bonded to four nitrogens so therefore an average valence of three is preserved. With the others, we now have two types of tetrahedra with average valence 11/4 (Ga_3Zn, Zn_2GeGa) and two with average valence 13/4 (Ga_3Ge, $ZnGe_2Ga$). One can think of these as acceptor- or donor-type deviations from the octet rule, respectively. Neither of these structures has any symmetry elements.

Finally, in Fig. 3 we illustrate that one can construct superlattices in the b direction with arbitrary arrangements of GaN and $ZnGeN_2$ half-unit cells and thus obtain other compositions in the alloy system $(ZnGeN_2)_x(GaN)_{2(1-x)}$.

B. Structural relaxation and energies of mixing

The relaxed lattice parameters of the $ZnGeGa_2N_4$ structures presented in Sec. III A are summarized in Table I. For completeness, we also recalculated GaN and $ZnGeN_2$ with the same approach. All results here were obtained first within the LDA. We note that the b/a and c/a ratios for

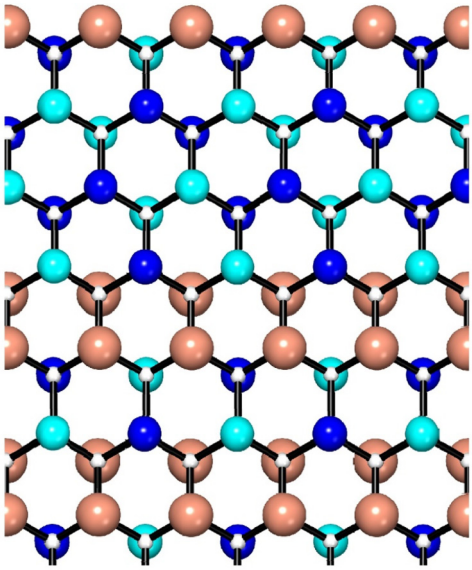

FIG. 3. Example of a superlattice arrangement of alternating $ZnGeN_2$ and GaN units.

$ZnGeGa_2N_4$ are somewhat closer to those of GaN and larger than for $ZnGeN_2$. The volume per 16-atom unit cell is close to the average volume of $ZnGeN_2$ and GaN, which is 171.3, indicating that Vegard's law is obeyed in this alloy system. We further see that the two octet-rule-preserving structures have very close b/a and c/a ratios and also approximately the same volume, to within 1 $Å^3$. The lattice constant mismatch between $ZnGeN_2$ and GaN in the LDA is about 2%. This appears to be somewhat larger than the experimental lattice mismatch [9,54]. Within the GGA-PBE, we can see that the lattice volumes are significantly closer, to less than 0.15% and hence the average lattice constants ($V^{1/3}$) differ by less than 0.05%. Even, so the mixed $ZnGeGa_2N_4$ compound is still found to have very close to the average of the $ZnGeN_2$ and GaN volumes, and Vegard's law is still obeyed. The optimum volume per cell in the GGA approximations is 11% larger than in the LDA. This ratio of GGA/LDA volume is similar to the one obtained previously for $ZnGeN_2$ [11]. In that case, the experimentally determined volume was found to be about halfway in between. Thus we expect the GGA and LDA to be upper and lower limits to the true lattice volume. The reduced coordinates for the atoms in the $Pmn2_1$ structure are included in Table II (and for $P1n1$, in Table III), while for the $[100]_{1/2}$ and $[001]_{1/2}$ superlattices they are provided in the Supplemental Material [55].

We now discuss the stability of the new compound. First, we find the cohesive energy, that is, the absolute value of the total energy per formula unit (f.u.) ($ZnGeGa_2N_4$) minus those of the corresponding free atoms. For the $Pmn2_1$ structure, which has the lowest total energy, this value is calculated to be $E_{coh} = 36.208$ eV/f.u. of eight atoms in LDA and 32.858 eV in GGA. This result corresponds to about 4.5 eV/atom in LDA (and 4.11 eV/atom in GGA), comparable to that of GaN, which is ~5.3 eV/atom (LDA) (4.43 eV in GGA). In fact, as we can see in Table IV which lists the more accurate GGA results, the value for $ZnGeGa_2N_4$ falls between those of GaN

TABLE I. Calculated structural parameters of the GaN, $ZnGeN_2$, and $ZnGeGa_2N_4$ structures in the LDA. For a few cases, GGA results are also shown.

Compound	Method	Space group	SL[a]	a (Å)	b (Å)	c (Å)	V[b] (Å^3)	b/a	c/a
GaN	LDA	$Pbn2_1$[c]		6.311	5.465	5.140	177.3	0.866[d]	0.8145
GaN	GGA	$Pbn2_1$		6.435	5.573	5.241	188.0	0.866	0.8145
$ZnGeN_2$	LDA	$Pbn2_1$		6.238	5.277	5.022	165.3	0.846	0.805
$ZnGeN_2$	GGA	$Pbn2_1$		6.499	5.504	5.248	187.7	0.847	0.8075
$ZnGeGa_2N_4$	LDA	$Pmn2_1$	$[010]_{1/2}$	6.231	5.365	5.072	169.6	0.861	0.814
$ZnGeGa_2N_4$	GGA	$Pmn2_1$		6.473	5.536	5.241	187.8	0.855	0.8097
$ZnGeGa_2N_4$	LDA	$P1n1$		6.240	5.369	5.077	170.1	0.860	0.814
$ZnGeGa_2N_4$	LDA	$P1$[e]	$[100]_{1/2}$	6.231	5.365	5.072	169.6	0.861	0.814
$ZnGeGa_2N_4$	LDA	$P1$	$[001]_{1/2}$	6.231	5.365	5.072	169.6	0.861	0.814

[a]Superlattice notation where applicable.
[b]Volume per 16-atom cell.
[c]The space group of wurtzite is $P6_3mc$ but we here give the parameters for the $Pbn2_1$ supercell for easy comparison to the other compounds.
[d]Equal to $\sqrt{3}/2$.
[e]For the last two structures, we assumed the same lattice constants as for $Pmn2_1$.

and $ZnGeN_2$. Here we have calculated the energies of the various free atoms using the same LDA (GGA) and including spin polarization for the atoms. These results are probably slightly overestimated because we did not here include the zero-point-motion correction of the solids or the molecule. The zero-point-motion correction for $ZnGeN_2$ amounts to only 78 meV/f.u., whereas for the N_2 molecule it is 146 meV.

Next, we consider the formation energy, which is the energy of the compound minus the sum of the energies of the corresponding atoms in their equilibrium phases at room temperature and pressure. This quantity is more difficult to calculate accurately because it requires comparable accuracies for each of the cohesive energies and thus absolute convergence with respect to **k**-point sets and other convergence parameters. We prefer here to use the GGA results. Using the GGA cohesive energies of Zn (−1.08 eV/atom), Ge (−4.49 eV/atom), Ga (−2.86 eV/atom) [19], and the binding energy of the N_2 molecule (−8.45 eV, in reasonable agreement with the experimental value of −9.91 eV), we obtain a formation energy of −4.668 eV/f.u. or −0.58/atom. The corresponding results for GaN and $ZnGeN_2$ are given in Table IV. The result for $ZnGeGa_2N_4$ is negative and in fact larger in absolute value than for $ZnGeN_2$, indicating that the compound should be thermodynamically stable. The zero-point-motion (ZPM) correction could reduce the formation energy because this correction is higher in the N_2 molecule than in the typical solids. Estimating the ZPM for $ZnGeGa_2N_4$ to be about twice that for $ZnGeN_2$, or ∼160 meV, we estimate that the formation energy could be further lowered by 0.22 eV per formula unit, a value which is negligible compared to the formation energy. We note that our result for $ZnGeN_2$ here is somewhat lower than in Ref. [19] because the structures were relaxed more accurately here. For GaN, the result is in good agreement with the experimental value of -1.70 ± 0.16 eV [56]. One could also consider the possibility of dynamical instability arising from soft phonons. This possibility is unlikely, however, given that the tetrahedrally bonded structure of $ZnGeGa_2N_4$ is very similar to those of $ZnGeN_2$ and GaN, which are both dynamically stable. Calculations of the phonons are postponed for later work.

Perhaps a more relevant quantity of interest is the mixing energy, often called mixing enthalpy, although we here do not include pressure effects. The mixing energy is defined by

$$N_{\text{cell}} E_{\text{mix}} = E_{\text{cell}}(\text{ZnGeGa}_2\text{N}_4) - \tfrac{1}{2} E_{\text{cell}}(\text{ZnGeN}_2) - \tfrac{1}{2} E_{\text{cell}}(\text{GaN}), \quad (2)$$

where the energies of each system are all calculated in a cell of the same total number of atoms $N_{\text{cell}} = 16$. The mixing energy per atom obtained in GGA amounts to 66 meV. The positive value implies that this compound wants to phase separate into GaN and $ZnGeN_2$. Extrapolating this result to the alloys, and assuming that these are close enough to equilibrium to

TABLE II. Reduced coordinates of atoms for the $Pmn2_1$ structure.

Atom	Wyckoff[a]	x	y	z
Ga	4b	0.2502	−0.3304	0.5000
Zn	2a	0.0000	0.1657	0.5000
Ge	2a	0.0000	−0.1663	0.0000
N_{Ga}	4b	0.2410	−0.3304	0.8781
N_{Zn}	2a	0.0000	0.1561	0.8820
N_{Ge}	2a	0.0000	−0.1733	0.3634

[a]2a positions are $(0, y, z)$ and $(1/2, -y, z + 1/2)$, 4b positions are (x, y, z), $(-x + 1/2, -y, z + 1/2)$, $(x + 1/2, -y, z + 1/2)$, and $(-x, y, z)$.

TABLE III. Reduced coordinates of atoms for the $P1n1$ structure.

Atom	Wyckoff[a]	x	y	z
Ge	2a	0.0001	−0.1676	−0.0057
Zn	2a	0.2496	0.3317	−0.0079
Ga_1	2a	0.4998	−0.1645	−0.0065
Ga_2	2a	0.7504	0.3345	−0.0069
N_{Ge}	2a	0.0034	−0.1687	0.3573
N_{Zn}	2a	0.2567	0.3303	0.3779
N_{Ga1}	2a	0.4965	−0.1554	0.3710
N_{Ga2}	2a	0.7434	0.3244	0.3707

[a]All atoms in 2a positions: (x, y, z), $(x + 1/2, -y, z + 1/2)$.

TABLE IV. Cohesive energies, energies of formation, and mixing energies in GGA.

	GaN	$ZnGeN_2$	$ZnGeGa_2N_4$ ($Pmn2_1$)
E_{coh} (eV/atom)	4.43	3.92	4.11
E_{for} (eV/atom)	−0.89	−0.41	−0.58
E_{mix} (meV/atom)			66.3

only contain octet-rule-obeying structures, we may estimate a corresponding miscibility gap temperature. Within a regular solution model, the miscibility gap temperature T_{MG}, which is the maximum of the miscibility dome, is then given by $T_{MG} = 2E_{mix}/k_B$ with k_B Boltzmann's constant. It is here found to be about 1500 K. This result is larger than typical growth temperatures of these materials. However, it does not quite preclude the possibility of growing such an alloy system because many growth methods are somewhat out of equilibrium. In fact, most semiconductor alloy systems are in principle phase separating, but this situation has not prevented researchers from designing and growing intricate mixed heterostructures based on such alloys. We note that the miscilibity gap is essentially a thermodynamic equilibrium concept.

Finally, we examine the relative energies of the different structures for $ZnGeGa_2N_4$ in Table V. We can see that the two structures which obey the octet rule are close to each other in total energy, to within about 0.2 eV/f.u., whereas the ones that break the octet rule are both higher in energy by ∼3 eV. Per atom this amounts to 23 meV for the two octet-rule-obeying structures, and ∼0.4 eV/atom for the octet-rule-violating ones, or about 20 times larger for the latter.

C. Predicted XRD spectra

In Fig. 4 we show the simulated XRD spectra of the two octet-rule-obeying structures compared with those of wurtzite GaN and $Pbn2_1$ $ZnGeN_2$. These are calculated at the LDA lattice constants and using the relaxed structures. We see that the main peaks of wurtzite GaN are shared with the other structures, although the peak positions are somewhat different, reflecting the different lattice constants. In the low-angle region, several much smaller superlattice peaks can be found which distinguish the different orderings. In addition, several splittings of the main peaks occur due to the deviations from the perfect hexagonal structure b/a ratio. For example, we see that the peaks near 32°, 37°, 48°, 58°, and 64° in $ZnGeN_2$ are split in comparison to the corresponding peaks in GaN. These peaks are also split in $ZnGeGa_2N_4$ but the splitting is smaller.

TABLE V. Energy differences of different structures of $ZnGeGa_2N_4$ per formula unit relative to the lowest energy structure.

Structure	ΔE (eV)
$Pmn2_1$	0
$P1n1$	0.182
$[100]_{1/2}$	3.220
$[001]_{1/2}$	2.914

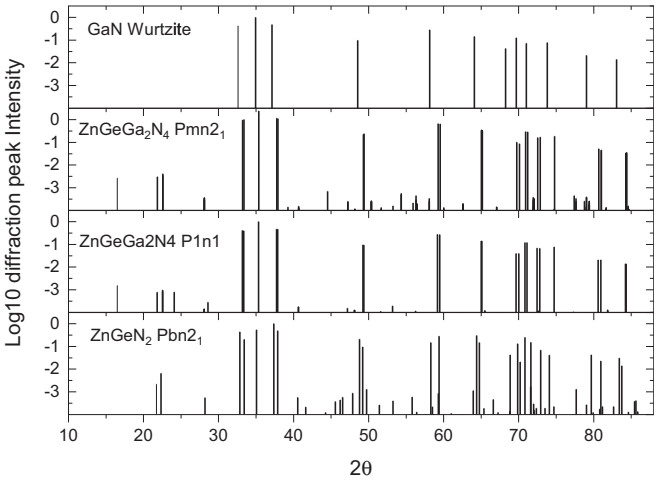

FIG. 4. Simulated XRD spectra of the GaN, $Pmn2_1$ and $P1n1$ $ZnGeGa_2N_4$, and $Pbn2_1$ $ZnGeN_2$.

At high angles, we see that sufficient differences exist to allow one readily to distinguish the different orderings.

D. Electronic band structure

In Fig. 5 we show the band structure and density of states of $ZnGeGa_2N_4$ in the lowest total energy $Pmn2_1$ structure obtained within the 0.8Σ approximation. We can see that the band gap is direct at Γ, as is also the case for $ZnGeN_2$ and GaN. The VBM is relatively flat while the CBM shows a small effective mass, similar to that in GaN or $ZnGeN_2$. We can recognize the Zn-3d bands at about −10 eV relative to the VBM. The Ge-3d and Ga-3d semicore states are not shown but occur at about −30 and −20 eV, respectively, the latter overlapping with the N-2s band, which ranges from about −20 to −15.5 eV. The partial densities of states show that the conduction band minimum has strong Ga-4s and Ge-4s character antibonding with N-2p but less Zn-4s. A more detailed evaluation [55] shows that the CBM at Γ has about half the amount of Ge-s character compared to Ga-s and negligible Zn-s. The percentages of cation content are 32% Ge-s, 63% Ga-s, and 5% Zn-s. The GW corrections to these bands are substantial. We will mainly focus on the bands near the gap where the self-energy shift corresponds more or less to a rigid shift with respect to LDA.

A zoom in on the band structure near the gap region is shown for the two octet-rule-preserving structures in Fig. 6. We can see very little difference between the conduction bands of these two band structures, or between these and that of the $[001]_{1/2}$ structure. Therefore, the band structure of the latter is not shown here. It is available in the Supplemental Material [55]. For the $[100]_{1/2}$ structure we can see a much flatter highest valence band near Γ and different splittings of the VBM at Γ.

Next, we present the band gaps in various approximations and for various structures in Table VI. The values here for $ZnGeN_2$ do not include the estimated zero-point-motion corrections or exciton effects, which were included in Punya *et al.* [1] and amount to about 0.12 eV but otherwise agree pretty closely, although slightly better-converged basis set

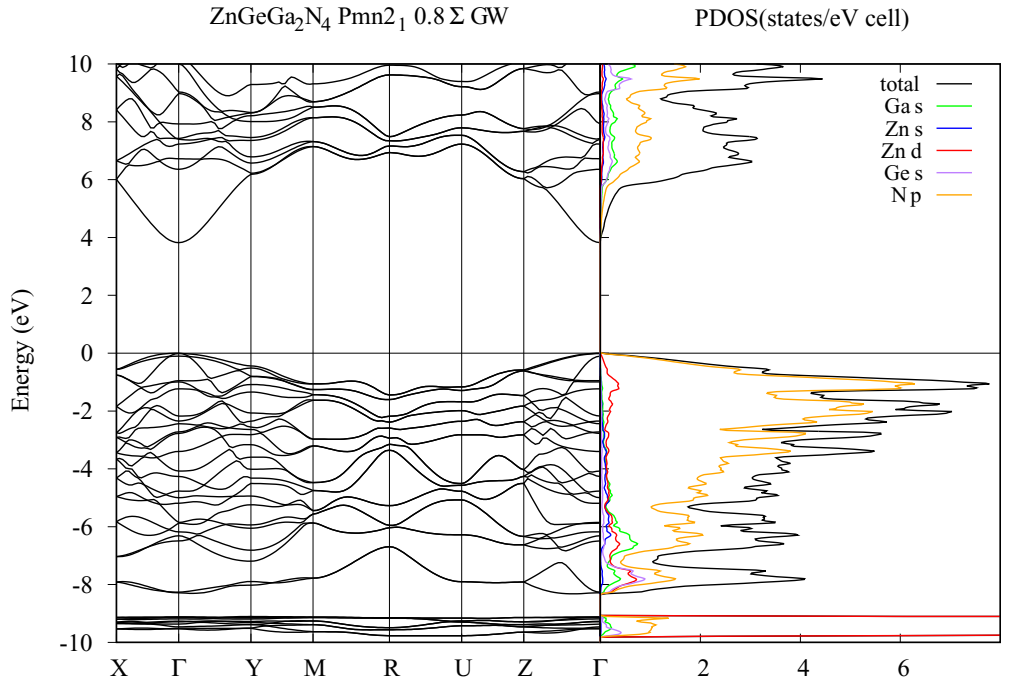

FIG. 5. Electronic band structure and partial densities of states for $ZnGeGa_2N_4$ in the $Pmn2_1$ structure within the 0.8Σ approximation.

parameters were used here compared to the earlier work. Another difference between this and the earlier work is that here all are evaluated at the LDA volume, which is slightly smaller than the experimental volume used previously. Use of the smaller volume will tend to increase the gap. The experimental gap of $ZnGeN_2$ at low temperature was measured to be 3.4 eV [9]. Within the precision of about 0.1 eV, we can see that the gap of GaN and $ZnGeN_2$ are the same. The gap of the $ZnGeGa_2N_4$ structure is slightly higher in the $Pmn2_1$ structure and even higher in the $P1n1$ structure but lower than that of $ZnGeN_2$ in the $[100]_{1/2}$ structure and also smaller, but less so, in the $[001]_{1/2}$ structure. We can see that most of these variations are already contained in the LDA gaps. In other words, the GW correction is almost constant throughout this family. A possible reason for the lower gap in the $[100]_{1/2}$ case will be discussed in the next section.

Because the two octet-rule-preserving structures we considered here differ in total energy by only ∼20 meV/atom, which is small considering the typical growth temperature, one might expect in an alloy close to equilibrium to find some disordered mixture of both of these type of structures. The octet-rule-violating structures, however, have significantly higher energy and may thus, to first approximation, be ignored, suggesting that the gaps will lie between 3.8 and 4.2 eV. Thus we expect that these alloys could in fact be used to extend the gap toward higher values, deeper into the UV, rather than toward smaller gaps as we anticipated in the Introduction. On the other hand, if octet-rule-violating local configurations are somehow frozen in kinetically, then lower gaps could occur. Modeling of fully random alloys is not attempted in this work.

Finally, as noted earlier, LDA underestimates the lattice constants. With the larger GGA volume, we find the 0.8Σ gap of the $Pmn2_1$ structure to be 3.16 eV instead of 3.82 eV. This gap change, due to the different lattice constants, is already present at the LDA level. It indicates a band gap deformation potential $dE_g/d\ \ln V \approx -6$ eV. This result is again similar to that for $ZnGeN_2$. Taking the average of the LDA and GGA as our best estimate of the lattice volume, we may expect a gap of 3.49 eV. This value is slightly larger than the experimental value of the $ZnGeN_2$ gap of 3.4 eV.

TABLE VI. Band gaps in eV for different compounds and structures and in different approximations, all calculated at the LDA relaxed volume.

Compound	Structure	LDA	QSGW	0.8Σ
GaN	Wurtzite	2.12	3.93	3.57
$ZnGeN_2$	$Pbn2_1$	2.20	4.02	3.66
$ZnGeGa_2N_4$	$Pmn2_1$	2.33	4.20	3.82
	$P1n1$	2.24	4.47	4.24
	$[100]_{1/2}$	1.73	3.69	3.28
	$[001]_{1/2}$	2.15	4.11	3.7

E. Discussion

1. Size quantization

Here we discuss the somewhat surprising result that the gap is found to be larger in $ZnGeGa_2N_4$ than in $ZnGeN_2$ or GaN, rather than lower, as might be anticipated from the type-II band offset. As mentioned in Sec. III A, the $Pmn2_1$ structure can be viewed as an extremely thin superlattice $[010]_{1/2}$ of $ZnGeN_2$ and GaN. Because of the type-II band offset, we can think of this structure as a superlattice with electron quantum wells in the GaN region and hole quantum wells in the $ZnGeN_2$ region. While the type-II offset suggests

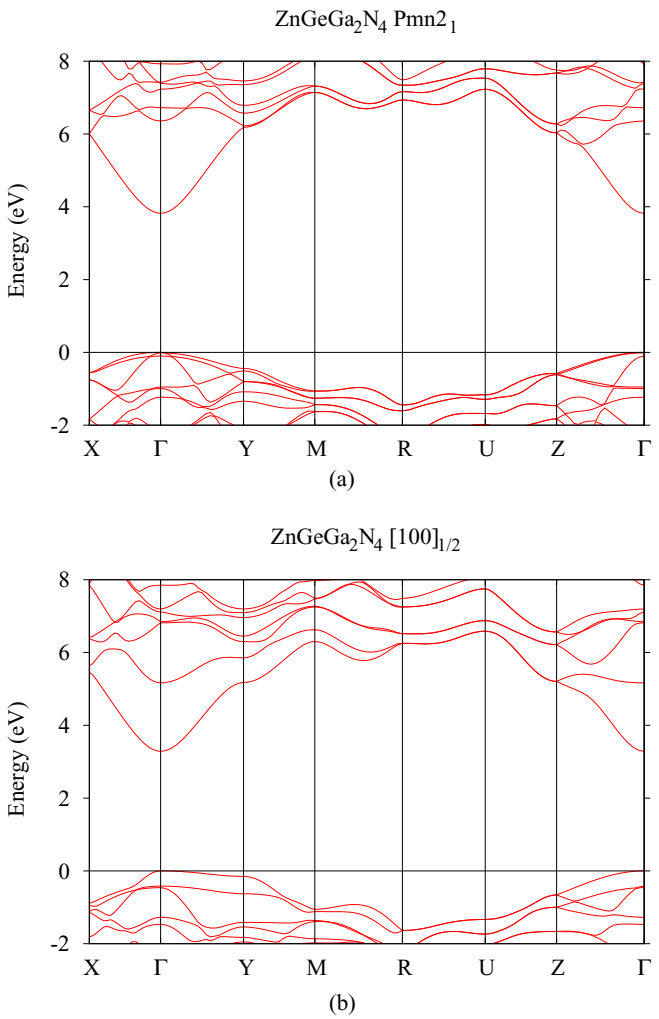

FIG. 6. Zoom in on the band structures near the gap region in (a) $Pmn2_1$ and (b) $[100]_{1/2}$ structures.

the bottom of the GaN well is then separated from the top of the $ZnGeN_2$ VBM well by the interface gap $E_g - \Delta E_v$ with ΔE_v the valence band offset, we need to now also consider the size quantization effects in each well. Obviously, these will increase the effective gap. Because a finite quantum well has always at least one bound state, the lowest quantized level in the GaN quantum well could occur at most at the position of the $ZnGeN_2$ CBM, and likewise for the holes. Thus, under extreme quantization, the gap could be as large as $\Delta E_g + \Delta E_v$, or 4.8 eV.

We can make an estimate of the size quantization using a Kronig-Penney model, assuming the same conduction band mass of $0.2m_e$ for $ZnGeN_2$ [1] and GaN [57], a well width of $b/2 \approx 2.68$Å, and a barrier height of $\Delta E_v = 1.2$ eV [33]. This gives the lowest conduction band in the well at $\delta E_c = 0.59$ eV above the GaN CBM bottom of the well. Similarly, for the holes in the $ZnGeN_2$ wells, we use an effective mass of 1.35 and obtain a quantized level at $\delta E_v = -0.52$ eV. The effective gap of the structure is then predicted to be $E_g - \Delta E_v + \delta E_c - \delta E_v \approx 3.5$ eV. This value is close to the gap of the two separate materials, indicating that size quantization effects play a significant role. Of course this

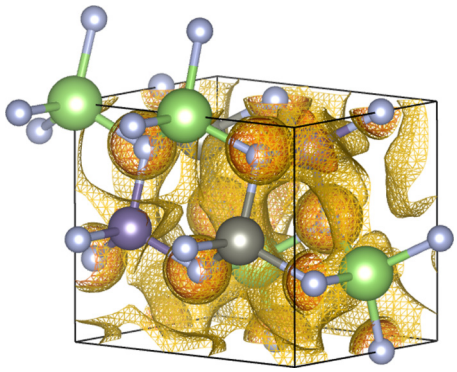

FIG. 7. Conduction band minimum wave function squared, at Γ, shown as two isosurfaces in the form of a wire mesh with specific colors: the darker core colored isosurface is primarily centered around the nitrogen atoms and corresponds to a value of 0.003 while the lighter yellow surface corresponds to a value of 0.001. Only the smooth part of the wave function squared is included in the calculation.

is an oversimplified model and one should not expect the continuum Kronig-Penney model to remain valid at such short length scales. Nonetheless, this picture explains qualitatively why the gap in the mixed structures is within ±0.1 eV of that of its components. The size quantization effects almost perfectly cancel the reduced gap due to the staggered band offset.

As a result, we expect the CBM wave function not to be confined to the Ga atoms but to spread around the Ga and Ge atoms. As we noted earlier, the CBM in the $ZnGeN_2$ is more Ge- than Zn-like but in both materials it also has a strong N contribution because it is an antibonding state with N-s. We attempt to visualize this wave function by plotting an isosurface of the CBM state at Γ in Fig. 7. One can see that the smaller isosurface value encompasses the Ge (purple) as well as the Ga (green) atoms but not the Zn atom (gray) and has also a large contribution in the interstitial region. This picture illustrates that this state extends throughout the cell rather than being confined to the GaN region.

One may now argue that, in the $P1n1$ structure, the size quantization effect could be even stronger as the atoms are intermixed at an even smaller length scale, and thus could at least qualitatively explain the slightly larger gap. On the other hand, when considering the $[100]_{1/2}$ superlattice, two effects come into play: first the well width is now somewhat larger and second, the band offset is predicted to be slightly larger in this direction. Both effects would tend to make the gap smaller. The Kronig-Penney model, however, is not accurate enough in its predictions to quantitatively explain the differences in gaps. On the other hand, we now have octet-rule-violating tetrahedra. One could view these as introducing Ga_{Ge}-like acceptor and Ga_{Zn}-like donor states [15]. Both are relatively shallow defects, especially the donors, but could nonetheless be viewed as reducing the gap. Why this effect is stronger for the $[100]_{1/2}$ than for the $[001]_{1/2}$ cells is not clear but we note that the difference in the band offsets is mainly between [100] and the other two directions [010] and [001], which have almost equal band offsets. Finally, we caution

here that the band offsets have not yet been confirmed by experiment.

2. Comparison with experiment

Here we discuss briefly how our work relates to the recent experimental work on mixed $ZnGeN_2$-GaN alloys [38]. That paper appears to reach rather different conclusions than one would predict from the work presented here: first, beyond 10% Ga, they find the cations disorder completely, thus giving rise to a disordered wurtzite structure. This result would suggest that the local octet rule, which we find to be very important for energetic stability, does not play much of a role in this material. This result may be a result of the synthesis method, which starts from oxide powder mixtures which are then exposed to a gas reduction nitridation reaction, and which could potentially yield structures far from equilibrium. Even for pure $ZnGeN_2$, the order-disorder question is a subtle one and obtaining well-ordered cations in the $Pbn2_1$ structure depends senstitively on the growth temperature, which needs to be sufficiently high to allow surface diffusion during growth to reach equilibrium. Specifically, it was reported by Blanton *et al.* [10,58] that ordered $Pbn2_1$ $ZnGeN_2$ was obtained above 850 °C, whereas disordered wurtzitelike $ZnGeN_2$ was obtained at 750 °C. These values pertain to a specific vapor-liquid-solid growth method but more generally indicate that achieving ordered structures in these ternary systems, and therefore even more so in quaternary systems, is far from trivial. Furthermore, the observation of a wurtzitelike XRD may not necessarily indicate full disorder of the cations but may also arise from a polytypelike disorder among different stackings of octet-rule-preserving local motifs, as we found to be the case in $ZnSnN_2$ [12].

Secondly, Suehiro *et al.* [38] find band gaps less than those of $ZnGeN_2$ and GaN, as small as 3.02 eV at 50%, and ascribe this result to the staggered band offset [32], as was our own initial guess. In fact, they do not find the gradual change in gap with composition that one would expect for an alloy system but rather an abrupt decrease in gap from 3.42 eV at 0% GaN to 3.04 eV at 10%, and to 3.02 eV at 50%. This trend may indicate that the reduction in the gap that they observe is more related to octet-rule-violating disorder than to the incorporation of Ga. Our findings for the octet-rule-violating structures examined here agree qualitatively with the reduced gaps that they observe.

IV. CONCLUSIONS

In this paper we considered the possibility of $ZnGeN_2$-GaN alloys and more specifically an ordered new compound at the 50% composition. We find that octet-rule-preserving mixed structures are possible as polytypelike superlattices in the [010] direction of the $Pbn2_1$ structure of $ZnGeN_2$, where we may consider the elementary blocks or layers to be as small as half a $ZnGeN_2$ cell. Most of the paper focused on the 50% composition $ZnGeGa_2N_4$. Besides the above structure, one other octet-rule-preserving structure was found and two other octet-rule-violating structures were considered. The space groups of these structures were determined and their structures relaxed. The main conclusions were that the two octet-rule-preserving structures have significantly lower energy than the two octet-rule-violating structures, and had similar total energies, to within about 20 meV/atom. This mixed compound is found to have a negative energy of formation and is thus in principle thermodynamically stable with respect to the constituent elements. However, even the lowest energy $Pmn2_1$ structure of the mixed $ZnGeGa_2N_4$ is found to have higher energy than the two separate phases: the mixing energy is slightly positive. This result indicates a tendency toward phase separation. The band gap of the mixed system, evaluated using the QSGW method, was found to be close to but slightly larger than those of $ZnGeN_2$ and GaN for the low total energy octet-rule-preserving structures. This result indicates that the size quantization largely compensates the reduced gap expected from the staggered band offset, as explained qualitatively in terms of a Kronig-Penney model. The octet-rule-violating structures had slightly smaller gaps than the octet-rule-preserving ones, and in one case, the $[100]_{1/2}$ superlattice, the gap was smaller than the gaps of the two separate compounds. However, such octet-rule-violating structures are strongly disfavored from forming in equilibrium because of their significantly higher energy.

ACKNOWLEDGMENTS

This work was supported by the National Science Foundation, Division of Materials Research, under Grant No. 1533957. Calculations made use of the High Performance Computing Resource in the Core Facility for Advanced Research Computing at Case Western Reserve University.

[1] A. Punya, W. R. L. Lambrecht, and M. van Schilfgaarde, Phys. Rev. B **84**, 165204 (2011).
[2] T. R. Paudel and W. R. L. Lambrecht, Phys. Rev. B **78**, 115204 (2008).
[3] T. R. Paudel and W. R. L. Lambrecht, Phys. Rev. B **79**, 245205 (2009).
[4] M. Hagemann, C. Bhandari, and W. R. Lambrecht, Solid State Commun. **233**, 46 (2016).
[5] A. P. Jaroenjittichai and W. R. L. Lambrecht, Phys. Rev. B **94**, 125201 (2016).
[6] S. Pramchu, A. P. Jaroenjittichai, and Y. Laosiritaworn, in *Proceedings of the 10th Asian Meeting on Electroceramics (AMEC 10)* [Ceram. Int. **43**, S444 (2017)] .
[7] S. Lyu and W. R. L. Lambrecht, Phys. Rev. Mater. **1**, 024606 (2017).
[8] S. Lyu and W. R. L. Lambrecht, J. Appl. Phys. **123**, 205701 (2018).
[9] K. Du, C. Bekele, C. C. Hayman, J. C. Angus, P. Pirouz, and K. Kash, J. Cryst. Growth **310**, 1057 (2008).
[10] E. W. Blanton, K. He, J. Shan, and K. Kash, J. Cryst. Growth **461**, 38 (2017).
[11] P. C. Quayle, K. He, J. Shan, and K. Kash, MRS Commun. **3**, 135 (2013).
[12] P. C. Quayle, E. W. Blanton, A. Punya, G. T. Junno, K. He, L. Han, H. Zhao, J. Shan, W. R. L. Lambrecht, and K. Kash, Phys. Rev. B **91**, 205207 (2015).

[13] T. J. Peshek, T. R. Paudel, K. Kash, and W. R. L. Lambrecht, Phys. Rev. B **77**, 235213 (2008).

[14] E. W. Blanton, M. Hagemann, K. He, J. Shan, W. R. L. Lambrecht, and K. Kash, J. Appl. Phys. **121**, 055704 (2017).

[15] D. Skachkov, A. Punya Jaroenjittichai, L.-y. Huang, and W. R. L. Lambrecht, Phys. Rev. B **93**, 155202 (2016).

[16] D. Skachkov, P. C. Quayle, K. Kash, and W. R. L. Lambrecht, Phys. Rev. B **94**, 205201 (2016).

[17] D. Skachkov and W. R. L. Lambrecht, Phys. Rev. Mater. **1**, 054604 (2017).

[18] N. L. Adamski, Z. Zhu, D. Wickramaratne, and C. G. Van de Walle, J. Appl. Phys. **122**, 195701 (2017).

[19] W. R. L. Lambrecht and A. Punya, in *III-Nitride Semiconductors and their Modern Devices*, edited by B. Gill (Oxford University Press, New York, 2013), Chap. 15, pp. 519–585.

[20] A. D. Martinez, A. N. Fioretti, E. S. Toberer, and A. C. Tamboli, J. Mater. Chem. A **5**, 11418 (2017).

[21] E. Arca, A. Fioretti, S. Lany, A. C. Tamboli, G. Teeter, C. Melamed, J. Pan, K. N. Wood, E. Toberer, and A. Zakutayev, IEEE J. Photovoltaics **8**, 110 (2018).

[22] A. N. Fioretti, A. Zakutayev, H. Moutinho, C. Melamed, J. D. Perkins, A. G. Norman, M. Al-Jassim, E. S. Toberer, and A. C. Tamboli, J. Mater. Chem. C **3**, 11017 (2015).

[23] S. Lany, A. N. Fioretti, P. P. Zawadzki, L. T. Schelhas, E. S. Toberer, A. Zakutayev, and A. C. Tamboli, Phys. Rev. Mater. **1**, 035401 (2017).

[24] T. Veal, N. Feldberg, N. Quackenbush, W. Linhart, D. Scanlon, L. Piper, and S. Durbin, Adv. Energy Mater. **5** 1501462 (2015).

[25] F. Alnjiman, S. Diliberto, J. Ghanbaja, E. Haye, S. Kassavetis, P. Patsalas, C. Gendarme, S. Bruyére, F. Cleymand, P. Miska, P. Boulet, and J. Pierson, Sol. Energy Mater. Sol. Cells **182**, 30 (2018).

[26] L. Lahourcade, N. C. Coronel, K. T. Delaney, S. K. Shukla, N. A. Spaldin, and H. A. Atwater, Adv. Mater. **25**, 2562 (2013).

[27] N. Feldberg, B. Keen, J. D. Aldous, D. Scanlon, P. A. Stampe, R. Kennedy, R. Reeves, T. D. Veal, and S. Durbin, in *Proceedings of the 2012 38th IEEE Photovoltaic Specialists Conference (PVSC '12)* (unpublished), pp. 002524–002527.

[28] T. Wang, C. Ni, and A. Janotti, Phys. Rev. B **95**, 205205 (2017).

[29] S. Chen, P. Narang, H. A. Atwater, and L.-W. Wang, Adv. Mater. **26**, 311 (2014).

[30] L. Han, K. Kash, and H. Zhao, J. Appl. Phys. **120**, 103102 (2016).

[31] R. Mélanie, H. Bérangère, and M. Patrice, Phys. Status Solidi RRL **12**, 1800173 (2018).

[32] A. Punya and W. R. L. Lambrecht, Phys. Rev. B **88**, 075302 (2013).

[33] A. P. Jaroenjittichai, S. Lyu, and W. R. L. Lambrecht, Phys. Rev. B **96**, 079907(E) (2017).

[34] A. Boonchun and W. R. L. Lambrecht, Phys. Rev. B **81**, 235214 (2010).

[35] A. Boonchun and W. R. L. Lambrecht, in *Oxide-Based Materials and Devices II*, edited by F. H. Teherani, D. C. Look, and D. J. Rogers, Proceedings of SPIE, 2011 (SPIE, Bellingham, 2011), Vol. 7940, p. 79400N.

[36] T. Omata, K. Tanaka, A. Tazuke, K. Nose, and S. Otsuka-Yao-Matsuo, J. Appl. Phys. **103**, 083706 (2008).

[37] T. Omata, M. Kita, K. Nose, K. Tachibana, and S. Otsuka-Yao-Matsuo, Jpn. J. Appl. Phys. **50**, 031102 (2011).

[38] T. Suehiro, M. Tansho, and T. Shimizu, J. Phys. Chem. C **121**, 27590 (2017).

[39] U. von Barth and L. Hedin, J. Phys. C **5**, 1629 (1972).

[40] J. P. Perdew, K. Burke, and M. Ernzerhof, Phys. Rev. Lett. **77**, 3865 (1996).

[41] See https://www.questaal.org/. Our *GW* implementation was adapted from the original ecalj package now at https://github.com/tkotani/ecalj/.

[42] M. Methfessel, M. van Schilfgaarde, and R. A. Casali, in *Electronic Structure and Physical Properties of Solids. The Use of the LMTO Method*, Lecture Notes in Physics, Vol. 535, edited by H. Dreyssé (Springer-Verlag, Berlin, 2000), p. 114.

[43] T. Kotani and M. van Schilfgaarde, Phys. Rev. B **81**, 125117 (2010).

[44] R. Storn and K. Price, J. Global Optim. **11**, 341 (1997).

[45] X. Gonze, J. M. Beuken, R. Caracas, F. Detraux, M. Fuchs, G. M. Rignanese, L. Sindic, M. Verstraete, G. Zerah, and F. Jollet, Comput. Mater. Sci. **25**, 478 (2002).

[46] M. Fuchs and M. Scheffler, Comput. Phys. Commun. **119**, 67 (1999).

[47] M. van Schilfgaarde, T. Kotani, and S. V. Faleev, Phys. Rev. B **74**, 245125 (2006).

[48] T. Kotani, M. van Schilfgaarde, and S. V. Faleev, Phys. Rev. B **76**, 165106 (2007).

[49] L. Hedin, Phys. Rev. **139**, A796 (1965).

[50] L. Hedin and S. Lundqvist, in *Solid State Physics, Advanced in Research and Applications*, edited by F. Seitz, D. Turnbull, and H. Ehrenreich (Academic Press, New York, 1969), Vol. 23, pp. 1–181.

[51] C. Bhandari, M. van Schilgaarde, T. Kotani, and W. R. L. Lambrecht, Phys. Rev. Mater. **2**, 013807 (2018).

[52] A. N. Chantis, M. van Schilfgaarde, and T. Kotani, Phys. Rev. Lett. **96**, 086405 (2006).

[53] D. Deguchi, K. Sato, H. Kino, and T. Kotani, Jpn. J. Appl. Phys. **55**, 051201 (2016).

[54] T. Misaki, A. Wakahara, H. Okada, and A. Yoshia, J. Cryst. Growth **260**, 125 (2004).

[55] See Supplemental Material at http://link.aps.org/supplemental/10.1103/PhysRevMaterials.2.114602 for the Wyckoff positions for the $[100]_{1/2}$ and $[001]_{1/2}$ structures, zoom-in band structure figures, and an analysis of the Ge-*s*, Ga-*s*, and Zn-*s* orbital contributions to the bands.

[56] T. J. Peshek, J. C. Angus, and K. Kash, J. Cryst. Growth **311**, 185 (2008).

[57] A. Punya and W. R. L. Lambrecht, Phys. Rev. B **85**, 195147 (2012).

[58] E. Blanton, K. He, J. Shan, and K. Kash, in *Photovoltaic Technologies, Devices and Systems Based on Inorganic Materials, Small Organic Molecules and Hybrids*, MRS Proceedings Vol. 1493 (Materials Research Society, Pittsburgh, 2013), p. 237.